



Published in final edited form as:

Retina. 2019 March ; 39(3): 502–513. doi:10.1097/IAE.0000000000002027.

FREQUENT SUBCLINICAL MACULAR CHANGES IN COMBINED BRAF/MEK INHIBITION WITH HIGH-DOSE HYDROXYCHLOROQUINE AS TREATMENT FOR ADVANCED METASTATIC BRAF MUTANT MELANOMA:

Preliminary Results From a Phase I/II Clinical Treatment Trial

Akosua A. Nti, MD^{*}, Leona W. Serrano, BS^{*}, Harpal S. Sandhu, MD^{*}, Katherine E. Uyhazi, MD, PhD^{*}, Ilaina D. Edelstein, BA^{*}, Elaine J. Zhou, MD^{*}, Scott Bowman, MD^{*}, Delu Song, MD, PhD^{*}, Tara C. Gangadhar, MD[†], Lynn M. Schuchter, MD[†], Sheryl Mitnick, MPH, RN[†], Alexander Huang, MD[†], Charles W. Nichols, MD^{*}, Ravi K. Amaravadi, MD[†], Benjamin J. Kim, MD^{*}, and Tomas S. Aleman, MD^{*‡}

^{*}Department of Ophthalmology, Scheie Eye Institute at the Perelman Center for Advanced Medicine, University of Pennsylvania, Philadelphia, Pennsylvania

[†]Department of Medicine, Abramson Cancer Center, University of Pennsylvania, Philadelphia, Pennsylvania

[‡]Department of Ophthalmology Center for Advanced Retinal and Ocular Therapeutics, Perelman School of Medicine, University of Pennsylvania, Philadelphia, Pennsylvania

Abstract

Purpose—To assess the potential ocular toxicity of a combined BRAF inhibition (BRAFi) + MEK inhibition (MEKi) + hydroxychloroquine (HCQ) regime used to treat metastatic BRAF mutant melanoma.

Methods—Patients with stage IV metastatic melanoma and BRAF V600E mutations (n = 11, 31–68 years of age) were included. Treatment was with oral dabrafenib, 150 mg bid, trametinib, 2 mg/day, and HCQ, 400 mg to 600 mg bid. An ophthalmic examination, spectral domain optical coherence tomography, near-infrared and short-wavelength fundus autofluorescence, and static perimetry were performed at baseline, 1 month, and q/6 months after treatment.

Results—There were no clinically significant ocular events; there was no ocular inflammation. The only medication-related change was a separation of the photoreceptor outer segment tip from the apical retinal pigment epithelium that could be traced from the fovea to the perifoveal retina noted in 9/11 (82%) of the patients. There were no changes in retinal pigment epithelium melanization or lipofuscin content by near-infrared fundus autofluorescence and short-wavelength

Reprint requests: Tomas S. Aleman, MD, Perelman Center for Advanced Medicine, University of Pennsylvania, 3400 Civic Center Boulevard, Philadelphia, PA 19104; aleman@mail.med.upenn.edu.

None of the authors has any conflicting interests to disclose.

Supplemental digital content is available for this article. Direct URL citations appear in the printed text and are provided in the HTML and PDF versions of this article on the journal's Web site (www.retinajournal.com).

[ClinicalTrials.gov](https://clinicaltrials.gov) Identifier: NCT02257424.

fundus autofluorescence, respectively. There were no inner retinal or outer nuclear layer changes. Visual acuities and sensitivities were unchanged.

Conclusion—BRAFi (trametinib) + MEKi (dabrafenib) + HCQ causes very frequent, subclinical separation of the photoreceptor outer segment from the apical retinal pigment epithelium without inner retinal changes or signs of inflammation. The changes suggest interference with the maintenance of the outer retinal barrier and/or phagocytic/pump functions of the retinal pigment epithelium by effective MEK inhibition.

Keywords

MEK; hydroxychloroquine; interdigitation zone; outer segments; optical coherence tomography; central serous retinopathy; cutaneous melanoma; BRAF inhibition; MEK inhibition; photoreceptors; subretinal fluid

Metastatic cutaneous melanoma is a disease with a historically poor prognosis.^{1–4} Approximately half of patients with metastatic melanoma have mutations in *BRAF*, a gene that encodes a serine–threonine protein kinase that regulates cell proliferation, differentiation, and apoptosis pathways through activation of a mitogen-activated extracellular signal-regulated kinase (MEK).^{1,2,4–9} Initial success of BRAF inhibition for advanced *BRAF V600* mutant cutaneous melanoma was soon overshadowed by resistance.^{10–12} Combined MEK + BRAF inhibition was subsequently introduced to try to overcome treatment resistance, which resulted in significantly improved survival, although the anticancer efficacy is still hampered by heterogeneous mechanisms of resistance, such as autophagy.^{1,2,4,13–17}

Ocular side effects associated with MEK and BRAF inhibition, alone or in combination, are particularly concerning, as they can drastically impact the quality of life of patients benefitted by these life-prolonging treatments.^{18–20} As a class, MEK inhibitors (MEKi) have been linked to a number of ocular adverse events, such as neurosensory serous detachments, cystoid macular edema, retinal vein occlusions, retinal hemorrhages, and panuveitis.^{21–28} BRAF-inhibition (BRAFi), however, has shown predominance for abnormalities of the anterior segment including anterior uveitis, conjunctivitis, dry eye syndrome, episcleritis, blepharitis, and keratitis, with infrequent reports of posterior segment involvement as retinal vein occlusions.^{29–32} The increasing incidence of cutaneous melanoma and the prolonged life expectancy of patients as a result of the success of the new anticancer treatments may lead to an increased recognition of MEK-inhibitor associated retinopathies (MEKAR) as well as of retinal paraneoplastic syndromes.^{21–28,30–43} Hydroxychloroquine (HCQ), an autophagy inhibitor, has been used to potentiate the anticancer efficacy of MEKi + BRAFi in the treatment of metastatic mutant cutaneous melanomas.^{13,44–46} Adding HCQ, a potentially retinotoxic medication, however, poses additional concerns, especially at a time when the mechanisms mediating retinotoxicity associated with MEK and BRAF inhibition remain incompletely understood.^{43,47–49}

In this study, we prospectively monitored and analyzed in detail the retinal structure and function of the first 11 patients enrolled in an ongoing Phase I/II clinical trial that tested a combination of BRAFi + MEKi + HCQ as treatment for advanced metastatic mutant

melanoma. The goal was to assess the ocular safety profile of this new treatment combination and increase our understanding of the pathophysiology of the retinal changes associated with MEK + BRAF inhibition.

Methods

Patients with histopathologically confirmed stage IV metastatic melanoma and *BRAFV600E* mutations were enrolled in an open-label, Phase I/II clinical trial ([ClinicalTrials.gov](https://clinicaltrials.gov/ct2/show/study/NCT02257424) Identifier: NCT02257424). Treatment was with oral dabrafenib, 150 mg twice daily, trametinib, 2 mg daily, and HCQ, 400 mg to 600 mg twice daily. Anticancer therapies were allowed with the exception of other BRAF or MEK inhibitors. Patients were required to have discontinued active immunotherapy or chemotherapy at least 4 weeks before entering the study. First enrolled patient dosing took place on December 5, 2014, and recruitment continues. BRAFi/MEKi/HCQ medications were withheld in two patients after the 1 month visit because of systemic side effects (Table 1). The methodology described in this manuscript is limited to that needed for the longitudinal/prospective ocular evaluations and analyses performed at the University of Pennsylvania, one of the sites of this multiinstitutional study. Ocular toxicity was assessed at baseline, 1 month, and then every 6 months with a complete ophthalmic examination, central visual field sensitivity measurements and multimodal retinal imaging. Informed consent was obtained after explanation of the nature of the study; procedures complied with the Declaration of Helsinki and were approved by the institutional review board.

Visual acuity was measured with early treatment diabetic retinopathy study charts, color vision with the Farnsworth-Munsell dichotomous D15 test and visual sensitivities with light-adapted automatic perimetry using a conventional 10-2 testing protocol (size III white stimuli, full-thresholding strategy) (HFA II-i; Carl Zeiss Meditec, Dublin, CA). Spectral domain (SD) optical coherence tomography (OCT) and en face short-wavelength (SW) and near-infrared (NIR) fundus autofluorescence (FAF) imaging was performed with a scanning laser ophthalmoscope/OCT system (Software Version 6.0; Spectralis OCT/HRA, Heidelberg Engineering, Carlsbad, CA) system. Spectral domain OCT scanning was performed with 9 mm long horizontal sections crossing the anatomical fovea and with a 30° × 20° raster scan. Segmentation of SD-OCT images was performed with the built-in segmentation software of the OCT system supervised to ensure correct identification of the different laminar boundaries.⁵⁰ Retinal thickness was defined as the distance between the signal transition at the vitreoretinal interface (from the internal limiting membrane) and the posterior boundary of the major signal corresponding to the basal retinal pigment epithelium (RPE)/Bruch membrane complex (RPE/BrM). The outer nuclear layer was the major intraretinal hyporeflective signal bracketed between the outer plexiform layer and the external limiting membrane (ELM). The inner retinal thickness was defined as the distance between the internal limiting membrane and the outer plexiform layer.^{50,51} Longitudinal reflectivity profiles (LRPs) were generated at locations of interest using custom programs (MatLab 7.5; MathWorks) and ImageJ imaging analysis software (<http://imagej.nih.gov/ij/links.html>).⁵² Outer retinal sublaminae were defined as published.^{50,51,53} Longitudinal reflectivity profiles from a region extending 170 μm and centered at 0.5 mm and 1 mm of eccentricity nasal to the fovea were averaged.

Results

Eleven patients, ages 31 to 68 years with stage IV metastatic *BRAF V600E* mutant stage IV metastatic cutaneous melanoma, were included in this study (Table 1). Inclusion and exclusion criteria are listed in Supplemental Digital Content 1 (see Table 1, <http://links.lww.com/IAE/A806>). Ophthalmologic surveillance was required given the evidence of possible side effects existing at initiation of the study in 2014.³³ With the exception of one patient who was being treated for open-angle glaucoma, all subjects had a normal eye examination, visual acuity, visual fields, and retinal appearance on SD-OCT and en face imaging at baseline. Although the effects of the use of MEKi + BRAFi on the retina were expected to show a rapid onset, the examinations were planned not to burden these fragile patients.³² The compromise was to perform a detailed visual examination at baseline, one month posttreatment, and then every 6 months as long as there were no signs of concern. Patients were instructed to report if they had any changes in vision or ocular discomfort.

Transient Central Retinal Abnormalities

A faint deep yellowish lesion at the foveal center in both eyes was noted on the sixth patient (P6) enrolled in the study. The lesion left a circular area of NIR-hypoautofluorescence; SW-FAF was within normal limits (Figure 1A). At the fovea, there was elevation of the neurosensory retina with an intervening hyporeflective lesion between the ellipsoid zone (EZ) band and the RPE/BrM complex that may correspond to subretinal fluid (Figure 1B). Within this lesion, there was an amorphous hyperreflective signal. Interestingly, inspection of the parafoveal and perifoveal retina in this patient at this visit revealed that the interdigitation zone (IZ) between photoreceptor outer segment (POS) tip and the apical RPE appeared thicker and better defined above the RPE/BrM compared with baseline, which is better appreciated on magnified SD-OCT images (Figure 1C). The patient developed hyperpyrexia and general malaise and his BRAFi/MEKi/Hcq medications were withheld. An examination within 5 days of discontinuation, on his second posttreatment visit (V2) showed nearly total resolution of the structural changes and yellowish lesion, consistent with previously reported fast kinetics of this side effect.³²

Central Retinal Structure and Function During Treatment With MEKi + BRAFi + HCQ

At the time of recognition of the change in P6, reports on MEKi-associated retinal serous detachments and cystoid macular edema were beginning to emerge, which prompted a careful examination of each patient enrolled in this study.^{35,54} All patients remained visually asymptomatic. Visual acuity, central visual fields, and ocular examinations were unremarkable in all patients until the last available follow-up visit (Table 1). Two patients (P1 and P6) died of complications from their metastatic cancer and completed partial follow-up ophthalmic evaluations. Visual acuities and central field sensitivities by automated light-adapted static perimetry were not significantly different from baseline ($P < 0.05$). Color vision also remained normal 6 months after initiation of treatment in seven patients (P1, P2, P4, P6, P7, P8, and P10) tested. Close inspection of magnified SD-OCT cross-sections at the Visit 1 (V1) ~30 days posttreatment initiation compared with baseline disclosed a spectrum of changes that resembled milder forms of the abnormalities described in P6 (Figure 2A). The abnormalities, unlike those now recognized as MEKAR, could easily scape the trained

eye.³² Although the changes were most obvious at the foveal center, there was similar dissection between the IZ and RPE/BrM signal in the parafovea with the emergence of a well-defined IZ signal. The outer retinal lamination was otherwise undisturbed. Except for P6 where subretinal fluid was evident at the fovea, there was no evidence of obvious subretinal fluid or cystoid changes in any of the patients.

To localize the origin of the changes, LRPs from a location in the nasal parafovea were generated in each of the patients (Figure 2B). At baseline, the series of highly reflective bands that correspond to the ELM and signals distal to the ELM produce several peaks in the magnified LRPs (Figure 2B). Two inner peaks (1-ELM and 2-EZ) are clearly separated between well-defined troughs, whereas the other two peaks corresponding to the IZ and RPE/BrM appear as two peaks with an intervening shallow trough. At V1, the ELM and EZ signals are distanced from the RPE/BrM with the emergence of a clear trough between the IZ and RPE/BrM signal. In some patients, the LRPs waveform showed four clear peaks separated by three unmistakable troughs (Figures 2, P6, P5, P2, and P8). Interestingly, at 6 months, the LRP waveform reverted to baseline in some patients (e.g., Figures 2B, P6 and P5). Although the IZ band appears thickened in Figure 2A in most patients, the LRP segment that corresponds to the IZ signal appears to be unchanged in shape. There were no signs of ocular inflammation, pigment epithelial detachments, grossly distorted POSs, or obvious signs of subretinal accumulation of material. There were no reports of vision loss, ocular discomfort, or of visits to outside ophthalmologists because of ocular concerns in between the scheduled examinations.

Topography and Primary Site of the Outer Retinal Abnormalities

To determine the topographical distribution of the structural changes across the central retina, maps of the thickness of the EZ-to-RPE/BrM distance were generated for all patients at V1 and compared with baseline (Figure 3). Topography maps at baseline in the patients did not differ from normal subjects with slightly greater thicknesses inside 1.2 mm of the foveal center (normal mean \pm 2 SD = $45 \pm 3 \mu\text{m}$, $n = 73$) and thinner values at locations >1.2 mm from the foveal center with little variation in thickness ($39 \pm 2 \mu\text{m}$) with increasing distance from the foveal center. At V1, nearly all patients (except P1) showed increased EZ-to-RPE/BrM thickness at the fovea, with thickening extending mostly in the horizontal direction into the parafoveal and perifoveal retina. In some (P5, P6, and P8), there was some thickening extending into the superonasal quadrant. We next examined if there were any structural changes at the level of the RPE. For this, we used SW- and NIR-FAF which reflects the lipofuscin, melanin, and melanolipofuscin content within the RPE cells. There were no obvious changes on SW-FAF (see Figure 1, Supplemental Digital Content 2, <http://links.lww.com/IAE/A808>). Near-infrared FAF showed central hypoautofluorescence coinciding with the increased thickness of the EZ-to-RPE/BrM distance near the foveal center, which may reflect greater absorption of the infrared excitation light by the structural change occurring superficial to the RPE. The parafoveal–perifoveal retina showed a normal NIR-FAF appearance (see Figure 2, Supplemental Digital Content 3, <http://links.lww.com/IAE/A809>). These data suggest changes posttreatment were not limited to the foveal center, became less obvious over time, did not affect RPE melanization and likely did

not result in major dropout of POSs that would have resulted in changes in the lipofuscin content of the RPE detectable by SW-FAF.

The otherwise evenly laminated outer retina in the parafoveal region of patients demonstrating that the greatest changes in thickness were used to define the site of the primary abnormality. Longitudinal reflectivity profiles from the parafoveal location at V1 (Figure 4A, gray traces) were superimposed on LRPs from the same location obtained at baseline, before treatment initiation (Figure 4A, black traces). The first hyperreflective band superficial to the RPE's main peak has been attributed to the interdigitation of these two structures lending the OCT signal its conventional name of "IZ band."⁵⁵ The waveforms perfectly overlapped from the ELM to the IZ peak. A clear trough (Figure 4A, asterisks) deeper to the IZ signal clearly separated the IZ signal from a distanced RPE/BrM peak. The distance between the EZ and the IZ remained unchanged. The findings suggested that the parafoveal POS was unchanged and only distanced from the apical RPE, and demonstrated that the IZ band's signal is dominated by the POS tip and not by its interdigitation with the apical RPE.

We next tested the significance of the changes by focusing on comparisons of the foveal center and parafoveal (1.7 mm) locations in all patients compared with baseline using precise segmentations with the help of the LRPs generated at these locations. The thickness or distance between the EZ and the RPE/BrM interface as well as the distance between the EZ and the IZ were measured in all patients at the foveal center and in the parafoveal retina and plotted as a function of time after initiation of treatment (Figure 4, B and C). The EZ-to-RPE parameter represented the overall change in thickness, the EZ-IZ monitors a possible change in the POS length. At baseline, the EZ-to-RPE/BrM distance was within normal limits in all patients for both retinal locations. At V1, the EZ-to-RPE/BrM thickness became abnormally thick in 4/11 patients at the fovea and in 1/11 at the parafoveal location. The EZ-IZ distance was within normal limits in all patients and at both locations except for two patients (P5 and P8) who showed abnormal thickening at the foveal center. With continuous treatment, all values returned to normal limits at the V2 (180 days posttreatment). Although values could be within normal limits, there was a clear trend toward thicker values at V1 posttreatment. The change in thickness was then plotted as the difference between the posttreatment value and baseline measurements for each parameter and compared with the limits of the variation of the measurements as established in at least two independent SD-OCT scanning sessions in this cohort of patients at baseline and in normal subjects (Figure 4C). The graphs showed increased in EZ-to-RPE thickness compared with baseline for 9/11 patients at the foveal location and in 4/11 for the parafoveal retina with a return to baseline values at V2 in all but one patient (P4). The EZ-to-IZ distance was increased at the fovea in 4/11 patients but remained unchanged for all patients in the parafoveal retina. There were no significant changes in inner retinal thickness for any patient or retinal location.

Discussion

The treatment of cancer, in particular metastatic melanoma, is rapidly evolving with the recent introduction of molecularly targeted and immunomodulatory therapies.^{4,5} The ultimate success of such therapies depends on striking a balance between these life-

prolonging therapies and potentially serious adverse events that can force dose modification or interruption of treatments and impact the patient's quality of life. BRAF and MEK inhibition have been associated with potentially sight-threatening retinal side effects.^{18–32,56–59} In this study, HCQ, a known retinotoxic medication, was added to a combined treatment with dabrafenib (BRAFi) and trametinib (MEKi) in an effort to overcome treatment resistance.^{13,44–46,60} We conceived a protocol of ophthalmic monitoring that borrowed from the recommendations for the standard of care of patients with chronic exposure to HCQ and other retinotoxic agents.^{49,61} The goal was to provide a preliminary glimpse at the ocular safety profile of this new treatment combination and to evaluate the short-term risks of potentially sight-threatening complications that could impact the conduct of this trial. We found that BRAFi + MEKi + HCQ-associated retinal changes, mostly consisting of transient subclinical separation of the POS from the apical RPE across the macula, occurred at a similar frequency, and followed a similar timecourse of that reported in MEKAR, suggesting a common underlying mechanism.^{24,32,33,47} The results are also consistent with the low rate of clinically significant retinal toxicity reported by the largest studies of combined dabrafenib + trametinib therapy to date.^{35,54,62,63} There were no changes in vision and no evidence of ocular inflammation in any of the patients, contrasting with cases of symptomatic central serous chorioretinopathy reported in association with MEK inhibition and ocular inflammation after BRAF inhibition.^{1,27,31,33,62} We speculate that this specific combination (dabrafenib + trametinib + HCQ) may be associated with less frequent ocular side effects than other MEKi + BRAFi combinations.^{27,32,33} It is also possible that certain patients may be particularly prone to develop more severe abnormalities and that we, by chance, did not enroll such patients, an obvious limitation of this small study.³⁴ Longitudinal observations in larger groups of patients treated with this specific regime, evaluated in a similar manner and compared with appropriate controls are needed to confirm the prevalence and significance of these early observations.

The mechanisms by which MAPK/MEK inhibitors produce serous retinopathy remain to be elucidated.^{24,43,47–49} Separation of the tip of the POS from the apical RPE across the macula, with minor elongation of an otherwise normal appearing POSs observed in our study points to the RPE as the primary retinal target of the effects of the medications. We found no evidence of inner retinal thickening, which may be expected to occur if the inner retinal barrier became incompetent.⁶⁴ The changes instead suggest interference with the maintenance of the outer retinal barrier and/or phagocytic/pump function of the RPE. Involvement of aquaporin (AQP1) channels in RPE cells after MAPK-inhibition has been invoked as a possible mechanism of subretinal fluid accumulation.⁴⁷ However, recent *in vitro* experiments suggest that MEK-inhibition would cause upregulation of AQP1 channels and thus prevent, rather than cause, subretinal fluid accumulation.⁶⁵ Lengthening of the POS at the fovea in some patients suggests interference with the phagocytic and/or pump function of the RPE or POS renewal, as postulated for patients with drug-induced retinopathies, central serous chorioretinopathy, and forms of retinal degenerations.^{44,66–72} However, the confirmation of a normal POS structure and length in the perifoveal retina that showed the separation between the POS and the RPE is somewhat against this hypothesis. The subretinal material observed in P6 may represent unphagocytized POS because of a defective apposition of the apical RPE and the tip of the POS because of interposed fluid,

rather than a primary phagocytic defect.^{73,74} The predilection for the foveal region may be explained by increased functional load on foveal RPE cells imposed by higher photoreceptor-to-RPE cell ratios near the foveal center.⁷⁴ Abnormal maintenance of the outer retinal barrier and/or pump function of the RPE remain the most likely explanations.⁶⁴ Last, there is some evidence in support that antiretinal, anti-RPE, or antibestrophin antibodies triggered by MAP kinase inhibition may be responsible for melanoma-associated retinopathy with serous detachments as well as in acute exudative polymorphous vitelliform maculopathy, conditions that can share a similar, although not identical structural outcome.^{42,65,75} Animal experiments complemented by in vitro studies of the function of the RPE in relationship to the POS in the presence of each individual drug or combinations are needed to test these hypotheses.

The origin of the different outer retinal signals on SD-OCT has been subject to scrutiny because of the importance that the underlying structures have for vision.^{53,76} The signal attributed to the IZ corresponds to the contact cylinder of the POS, but there has been speculation as to whether this signal originates from light scattering from within the tip of the POS or by interaction with surrounding outer segments or melanin within the apical RPE.^{53,77,78} The emergence on longitudinal follow-up of a deeply hyporreflective signal between the parafoveal IZ band and the apical RPE with an otherwise intact retinal lamination in our patients presented a unique opportunity to reexamine the signal origin of the SD-OCT bands in the outer retina, particularly the IZ.^{52,53,55,77,79–86} The signal peak that corresponds to the IZ clearly separated from the RPE peak by a deep trough, adding support to the notion that the IZ band is dominated by signals originating from the POS tip.^{53,77,78} We could not discriminate between rod- versus cone-originated outer segment signals with the resolution of the system used in this work, and this may be a subject of further enquiry. The findings have implications beyond the academic exercise of signal origin analyses. By unambiguously placing the IZ signal at the POS tip, loss of the IZ signal in early stages of several retinal degenerations may be specifically linked to a POS abnormality and not be attributed to changes in the RPE, such as defects in RPE melanization, as may occur, for example, in albinism, choroideremia, and Bietti fundus dystrophy.^{50,87,88}

Normality of the RPE melanin and lipofuscin content in our patients as assessed with NIR- and SW-FAF, respectively, coupled with a normal photoreceptor structure and vision, supports no acute HCQ toxicity.⁴⁹ The magnitude and nature of the retinal changes observed in this study may be considered a transient modification of the retinal physiology rather than a bona fide adverse event with permanent sequelae. This preliminary analysis supports the retinal safety of this new treatment combination, but it may be still prudent to perform baseline and periodic evaluations, which may follow, at least initially, the standard of care recommendations for HCQ monitoring, a well known, although evolving model to assess medication-related retinotoxicity.⁴⁹ Although no obvious relationship has been found between the occurrence of clinically significant central serous chorioretinopathy and overall cancer survival, further studies are warranted to explore the utility of SD-OCT imaging and quantitation as an in vivo microscopic biomarker of effective MEK/BRAF inhibition.⁴⁷

Supplementary Material

Refer to Web version on PubMed Central for supplementary material.

Acknowledgments

Supported by grants from the National Institutes of Health (NEIK12EY015398-10), Hope for Vision, The Foundation Fighting Blindness, Macula Vision Research Foundation, The Paul and Evanina Bell Mackall Foundation Trust, The Pennsylvania Lions Sight Conservation and Research Foundation, and Research to Prevent Blindness.

Thanks are due to Grace Han and Lydia Giles for their critical help.

References

1. Flaherty KT, Robert C, Hersey P, et al. Improved survival with MEK inhibition in BRAF-mutated melanoma. *N Engl J Med*. 2012; 367:107–114. [PubMed: 22663011]
2. Pasquali S, Chiarion-Sileni V, Rossi CR, Mocellin S. Immune checkpoint inhibitors and targeted therapies for metastatic melanoma: a network meta-analysis. *Cancer Treat Rev*. 2017; 54:34–42. [PubMed: 28189914]
3. Eggermont AM, Spatz A, Robert C. Cutaneous melanoma. *Lancet*. 2014; 383:816–827. [PubMed: 24054424]
4. Ugurel S, Röhm J, Ascierto PA, et al. Survival of patients with advanced metastatic melanoma: the impact of novel therapies. *Eur J Cancer*. 2016; 53:125–134. [PubMed: 26707829]
5. Obaid NM, Bedard K, Huang WY. Strategies for overcoming resistance in tumours harboring BRAF mutations. *Int J Mol Sci*. 2017; 18doi: 10.3390/ijms18030585
6. Tran KA, Cheng MY, Mitra A, et al. MEK inhibitors and their potential in the treatment of advanced melanoma: the advantages of combination therapy. *Drug Des Devel Ther*. 2016; 10:43–52.
7. Davies H, Bignell GR, Cox C, et al. Mutations of the BRAF gene in human cancer. *Nature*. 2002; 417:949–954. [PubMed: 12068308]
8. Martin-Liberal J, Lagares-Tena L, Larkin J. Prospects for MEK inhibitors for treating cancer. *Expert Opin Drug Saf*. 2014; 13:483–495. [PubMed: 24597490]
9. Luke JJ, Flaherty KT, Ribas A, Long GV. Targeted agents and immunotherapies: optimizing outcomes in melanoma. *Nat Rev Clin Oncol*. 2017; 14:463–482. [PubMed: 28374786]
10. Gowrishankar K, Snoyman S, Pupo GM, et al. Acquired resistance to BRAF inhibition can confer cross-resistance to combined BRAF/MEK inhibition. *J Invest Dermatol*. 2012; 132:1850–1859. [PubMed: 22437314]
11. Rizos H, Menzies AM, Pupo GM, et al. BRAF inhibitor resistance mechanisms in metastatic melanoma: spectrum and clinical impact. *Clin Cancer Res*. 2014; 20:1965–1977. [PubMed: 24463458]
12. Lim SY, Menzies AM, Rizos H. Mechanisms and strategies to overcome resistance to molecularly targeted therapy for melanoma. *Cancer*. 2017; 123:2118–2129. [PubMed: 28543695]
13. Fennelly, C, Amaravadi, RK. Lysosomal biology in cancer. In: Öllinger, K, Appelqvist, H, editors. *Lysosomes*. Vol. 1594. New York, NY: Springer; 2017. 293–308.
14. Amaravadi RK, Thompson CB. The roles of therapy-induced autophagy and necrosis in cancer treatment. *Clin Cancer Res*. 2007; 13:7271–7279. [PubMed: 18094407]
15. Murugan S, Amaravadi RK. Methods for studying autophagy within the tumor microenvironment. *Adv Exp Med Biol*. 2016; 899:145–166. [PubMed: 27325266]
16. Yang ZJ, Chee CE, Huang S, Sinicrope FA. The role of autophagy in cancer: therapeutic implications. *Mol Cancer Ther*. 2011; 10:1533–1541. [PubMed: 21878654]
17. Gottlieb RA, Andres AM, Sin J, Taylor DPJ. Untangling autophagy measurements: all fluxed up. *Circ Res*. 2015; 116:504–514. [PubMed: 25634973]

18. Huillard O, Bakalian S, Levy C, et al. Ocular adverse events of molecularly targeted agents approved in solid tumours: a systematic review. *Eur J Cancer*. 2014; 50:638–648. [PubMed: 24256808]
19. Renouf DJ, Velazquez-Martin JP, Simpson R, et al. Ocular toxicity of targeted therapies. *J Clin Oncol*. 2012; 30:3277–3286. [PubMed: 22649132]
20. van der Noll R, Leijen S, Neuteboom GHG, et al. Effect of inhibition of the FGFR-MAPK signaling pathway on the development of ocular toxicities. *Cancer Treat Rev*. 2013; 39:664–672. [PubMed: 23434072]
21. Duncan KE, Chang LY, Patronas M. MEK inhibitors: a new class of chemotherapeutic agents with ocular toxicity. *Eye Lond Engl*. 2015; 29:1003–1012.
22. McCannel TA, Chmielowski B, Finn RS, et al. Bilateral subfoveal neurosensory retinal detachment associated with MEK inhibitor use for metastatic cancer. *JAMA Ophthalmol*. 2014; 132:1005–1009. [PubMed: 24852144]
23. Sheyman AT, Scarinci F, Fawzi AA, Gill MK. Long-term evaluation of MEK inhibitor retinal toxicity with multimodal imaging. *Ophthalmic Surg Lasers Imaging Retina*. 2016; 47:76–77. [PubMed: 26731214]
24. van Dijk EHC, van Herpen CML, Marinkovic M, et al. Serous retinopathy associated with mitogen-activated protein kinase kinase inhibition (Binimetinib) for metastatic cutaneous and uveal melanoma. *Ophthalmology*. 2015; 122:1907–1916. [PubMed: 26123090]
25. Avery RA, Trimboli-Heidler C, Kilburn LB. Separation of outer retinal layers secondary to selumetinib. *J AAPOS*. 2016; 20:268–271. [PubMed: 27108842]
26. Nolan DP, Lewis S, Hariprasad SM. Retinal toxicity associated with MEK inhibitor use for metastatic cancer: a rising trend in ophthalmology. *Ophthalmic Surg Lasers Imaging Retina*. 2016; 47:398–402. [PubMed: 27183542]
27. Weber ML, Liang MC, Flaherty KT, Heier JS. Subretinal fluid associated with MEK inhibitor use in the treatment of systemic cancer. *JAMA Ophthalmol*. 2016; 134:855–862. [PubMed: 27309887]
28. Alves C, Ribeiro I, Penedones A, et al. Risk of ophthalmic adverse effects in patients treated with MEK inhibitors: a systematic review and meta-analysis. *Ophthalmic Res*. 2017; 57:60–69. [PubMed: 27404571]
29. Choe CH, McArthur GA, Caro I, et al. Ocular toxicity in BRAF mutant cutaneous melanoma patients treated with vemurafenib. *Am J Ophthalmol*. 2014; 158:831–837. [PubMed: 25036880]
30. Welsh SJ, Corrie PG. Management of BRAF and MEK inhibitor toxicities in patients with metastatic melanoma. *Ther Adv Med Oncol*. 2015; 7:122–136. [PubMed: 25755684]
31. Dreno B, Ribas A, Larkin J, et al. Incidence, course, and management of toxicities associated with cobimetinib in combination with vemurafenib in the coBRIM study. *Ann Oncol*. 2017; 28:1137–1144. [PubMed: 28444112]
32. Urner-Bloch U, Urner M, Jaberg-Bentele N, et al. MEK inhibitor-associated retinopathy (MEKAR) in metastatic melanoma: long-term ophthalmic effects. *Eur J Cancer*. 2016; 65:130–138. [PubMed: 27497344]
33. Urner-Bloch U, Urner M, Stieger P, et al. Transient MEK inhibitor-associated retinopathy in metastatic melanoma. *Ann Oncol*. 2014; 25:1437–1441. [PubMed: 24864047]
34. Draganova D, Kerger J, Caspers L, Willermain F. Severe bilateral panuveitis during melanoma treatment by Dabrafenib and Trametinib. *J Ophthalmic Inflamm Infect*. 2015; 5:17. [PubMed: 26078801]
35. Long GV, Stroyakovskiy D, Gogas H, et al. Combined BRAF and MEK inhibition versus BRAF inhibition alone in melanoma. *N Engl J Med*. 2014; 371:1877–1888. [PubMed: 25265492]
36. Niro A, Strippoli S, Alessio G, et al. Ocular toxicity in metastatic melanoma patients treated with mitogen-activated protein kinase kinase inhibitors: a case series. *Am J Ophthalmol*. 2015; 160:959–967. [PubMed: 26231307]
37. Diem S, Keller F, Rüesch R, et al. Pembrolizumab-triggered uveitis: an additional surrogate marker for responders in melanoma immunotherapy? *J Immunother*. 2016; 39:379–382. [PubMed: 27662340]
38. Rocha Cabrera P, Quijada Fumero E, Losada Castillo MJ, et al. MEK Retinopathy. Clinical case reports. *Arch Soc Espanola Oftalmol*. 2017; doi: 10.1016/j.ofal.2017.03.005

39. Infante JR, Fecher LA, Falchook GS, et al. Safety, pharmacokinetic, pharmacodynamic, and efficacy data for the oral MEK inhibitor trametinib: a phase 1 dose-escalation trial. *Lancet Oncol.* 2012; 13:773–781. [PubMed: 22805291]
40. Stjepanovic N, Velazquez-Martin JP, Bedard PL. Ocular toxicities of MEK inhibitors and other targeted therapies. *Ann Oncol.* 2016; 27:998–1005. [PubMed: 26951625]
41. Schoenberger SD, Kim SJ. Bilateral multifocal central serous-like chorioretinopathy due to MEK inhibition for metastatic cutaneous melanoma. *Case Rep Ophthalmol Med.* 2013; 2013:673796. [PubMed: 23555064]
42. Sandhu HS, Kolomeyer AM, Lau MK, et al. Acute exudative paraneoplastic polymorphous vitelliform maculopathy during vemurafenib and pembrolizumab treatment for metastatic melanoma. *Retin Cases Brief Rep.* 2017; 1doi: 10.1097/ICB.0000000000000604
43. Merlino G, Herlyn M, Fisher DE, et al. The state of melanoma: challenges and opportunities. *Pigment Cell Melanoma Res.* 2016; 29:404–416. [PubMed: 27087480]
44. Ma XH, Piao SF, Dey S, et al. Targeting ER stress-induced autophagy overcomes BRAF inhibitor resistance in melanoma. *J Clin Invest.* 2014; 124:1406–1417. [PubMed: 24569374]
45. Galluzzi L, Bravo-San Pedro JM, Demaria S, et al. Activating autophagy to potentiate immunogenic chemotherapy and radiation therapy. *Nat Rev Clin Oncol.* 2017; 14:247–258. [PubMed: 27845767]
46. Ojha R, Amaravadi RK. Targeting the unfolded protein response in cancer. *Pharmacol Res.* 2017; 120:258–266. [PubMed: 28396092]
47. van Dijk EHC, Duits DEM, Versluis M, et al. Loss of MAPK pathway activation in post-mitotic retinal cells as mechanism in MEK inhibition-related retinopathy in cancer patients. *Medicine (Baltimore).* 2016; 95:e3457. [PubMed: 27149444]
48. Navajas EV, Krema H, Hammoudi DS, et al. Retinal toxicity of high-dose hydroxychloroquine in patients with chronic graft-versus-host disease. *Can J Ophthalmol.* 2015; 50:442–450. [PubMed: 26651304]
49. Marmor MF. Hydroxychloroquine screening alert: change is in the wind. *Ophthalmic Surg Lasers Imaging Retina.* 2017; 48:96–98. [PubMed: 28195610]
50. Aleman TS, Han G, Serrano LW, et al. Natural history of the central structural abnormalities in choroideremia: a prospective cross-sectional study. *Ophthalmology.* 2017; 124:359–373. [PubMed: 27986385]
51. Aleman TS, Cideciyan AV, Sumaroka A, et al. Retinal laminar architecture in human retinitis pigmentosa caused by Rhodopsin gene mutations. *Invest Ophthalmol Vis Sci.* 2008; 49:1580–1590. [PubMed: 18385078]
52. Huang Y, Cideciyan AV, Papastergiou GI, et al. Relation of optical coherence tomography to microanatomy in normal and rd chickens. *Invest Ophthalmol Vis Sci.* 1998; 39:2405–2416. [PubMed: 9804149]
53. Cideciyan AV, Hufnagel RB, Carroll J, et al. Human cone visual pigment deletions spare sufficient photoreceptors to warrant gene therapy. *Hum Gene Ther.* 2013; 24:993–1006. [PubMed: 24067079]
54. Robert C, Karaszewska B, Schachter J, et al. Improved overall survival in melanoma with combined dabrafenib and trametinib. *N Engl J Med.* 2015; 372:30–39. [PubMed: 25399551]
55. Spaide RF, Curcio CA. Anatomical correlates to the bands seen in the outer retina by optical coherence tomography: literature review and model. *Retina.* 2011; 31:1609–1619. [PubMed: 21844839]
56. Ascierto PA, McArthur GA, Dréno B, et al. Cobimetinib combined with vemurafenib in advanced BRAFV600-mutant melanoma (coBRIM): updated efficacy results from a randomised, double-blind, phase 3 trial. *Lancet Oncol.* 2016; 17:1248–1260. [PubMed: 27480103]
57. Liu CY, Francis JH, Brodie SE, et al. Retinal toxicities of cancer therapy drugs: biologics, small molecule inhibitors, and chemotherapies. *Retina.* 2014; 34:1261–1280. [PubMed: 24949716]
58. Francis JH, Habib LA, Abramson DH, et al. Clinical and morphologic characteristics of MEK inhibitor-associated retinopathy. *Ophthalmology.* 2017; 124:1788–1798. [PubMed: 28709702]
59. Larkin J, Ascierto PA, Dréno B, et al. Combined vemurafenib and cobimetinib in BRAF-mutated melanoma. *N Engl J Med.* 2014; 371:1867–1876. [PubMed: 25265494]

60. Shi TT, Yu XX, Yan LJ, Xiao HT. Research progress of hydroxychloroquine and autophagy inhibitors on cancer. *Cancer Chemother Pharmacol*. 2017; 79:287–294. [PubMed: 27889812]
61. Marmor MF, Kellner U, Lai TYY, et al. Recommendations on screening for chloroquine and hydroxychloroquine retinopathy (2016 Revision). *Ophthalmology*. 2016; 123:1386–1394. [PubMed: 26992838]
62. Flaherty KT, Infante JR, Daud A, et al. Combined BRAF and MEK inhibition in melanoma with BRAF V600 mutations. *N Engl J Med*. 2012; 367:1694–1703. [PubMed: 23020132]
63. Leijen S, Middleton MR, Tresca P, et al. Phase I dose-escalation study of the safety, pharmacokinetics, and pharmacodynamics of the MEK inhibitor RO4987655 (CH4987655) in patients with advanced solid tumors. *Clin Cancer Res*. 2012; 18:4794–4805. [PubMed: 22767668]
64. Cunha-Vaz, J. Mechanisms of retinal fluid accumulation and blood-retinal barrier breakdown. In: Coscas, G, Loewenstein, A, Cunha-Vaz, J, Soubrane, G, editors. *Developments in Ophthalmology*. Vol. 58. Basel, Switzerland: S. Karger AG; 2017. 11–20.
65. Jiang Q, Cao C, Lu S, et al. MEK/ERK pathway mediates UVB-induced AQP1 downregulation and water permeability impairment in human retinal pigment epithelial cells. *Int J Mol Med*. 2009; 23:771–777. [PubMed: 19424603]
66. Mannerström M, Mäenpää H, Toimela T, et al. The phagocytosis of rod outer segments is inhibited by selected drugs in retinal pigment epithelial cell cultures. *Pharmacol Toxicol*. 2001; 88:27–33. [PubMed: 11169158]
67. Herron WL, Riegel BW, Myers OE, Rubin ML. Retinal dystrophy in the rat—a pigment epithelial disease. *Invest Ophthalmol*. 1969; 8:595–604. [PubMed: 5359576]
68. Ojima Y, Hangai M, Sasahara M, et al. Three-dimensional imaging of the foveal photoreceptor layer in central serous chorioretinopathy using high-speed optical coherence tomography. *Ophthalmology*. 2007; 114:2197–2207. [PubMed: 17507096]
69. Matsumoto H, Kishi S, Otani T, Sato T. Elongation of photoreceptor outer segment in central serous chorioretinopathy. *Am J Ophthalmol*. 2008; 145:162–168. [PubMed: 18028861]
70. Matsumoto H, Kishi S, Sato T, Mukai R. Fundus autofluorescence of elongated photoreceptor outer segments in central serous chorioretinopathy. *Am J Ophthalmol*. 2011; 151:617–623. [PubMed: 21257153]
71. Wavre-Shapton ST, Calvi AA, Turmaine M, et al. Photoreceptor phagosome processing defects and disturbed autophagy in retinal pigment epithelium of *Cln3*^{ex1-6} mice modelling juvenile neuronal ceroid lipofuscinosis (Batten disease). *Hum Mol Genet*. 2015; 24:7060–7074. [PubMed: 26450516]
72. Mustafi D, Kevany BM, Genoud C, et al. Defective photoreceptor phagocytosis in a mouse model of enhanced S-cone syndrome causes progressive retinal degeneration. *FASEB J*. 2011; 25:3157–3176. [PubMed: 21659555]
73. Anderson DH, Fisher SK, Steinberg RH. Mammalian cones: disc shedding, phagocytosis, and renewal. *Invest Ophthalmol Vis Sci*. 1978; 17:117–133. [PubMed: 415019]
74. Volland S, Esteve-Rudd J, Hoo J, et al. A comparison of some organizational characteristics of the mouse central retina and the human macula. *PLoS One*. 2015; 10:e0125631. [PubMed: 25923208]
75. Crépel V, Panenka W, Kelly ME, MacVicar BA. Mitogen-activated protein and tyrosine kinases in the activation of astrocyte volume-activated chloride current. *J Neurosci*. 1998; 18:1196–1206. [PubMed: 9454830]
76. Hood DC, Zhang X, Ramachandran R, et al. The inner segment/outer segment border seen on optical coherence tomography is less intense in patients with diminished cone function. *Invest Ophthalmol Vis Sci*. 2011; 52:9703–9709.
77. Jonnal RS, Kocaoglu OP, Zawadzki RJ, et al. The cellular origins of the outer retinal bands in optical coherence tomography images. *Invest Ophthalmol Vis Sci*. 2014; 55:7904–7918. [PubMed: 25324288]
78. Gao W, Cense B, Zhang Y, et al. Measuring retinal contributions to the optical Stiles-Crawford effect with optical coherence tomography. *Opt Express*. 2008; 16:6486–6501. [PubMed: 18516251]

79. Flores M, DeBellemanière G, Bully A, et al. Reflectivity of the outer retina on spectral-domain optical coherence tomography as a predictor of photoreceptor cone density. *Am J Ophthalmol.* 2015; 160:588–595. [PubMed: 26095264]
80. Sampson DM, Alonso-Caneiro D, Chew AL, et al. Enhanced visualization of subtle outer retinal pathology by en face optical coherence tomography and correlation with multi-modal imaging. *PLoS One.* 2016; 11:e0168275. [PubMed: 27959968]
81. Wilk MA, Wilk BM, Langlo CS, et al. Evaluating outer segment length as a surrogate measure of peak foveal cone density. *Vis Res.* 2017; 130:57–66. [PubMed: 27887888]
82. Wilk MA, McAllister JT, Cooper RF, et al. Relationship between foveal cone specialization and pit morphology in albinism. *Invest Ophthalmol Vis Sci.* 2014; 55:4186–4198. [PubMed: 24845642]
83. Panorgias A, Zawadzki RJ, Capps AG, et al. Multimodal assessment of microscopic morphology and retinal function in patients with geographic atrophy. *Invest Ophthalmol Vis Sci.* 2013; 54:4372–4384. [PubMed: 23696601]
84. Jonnal RS, Besecker JR, Derby JC, et al. Imaging outer segment renewal in living human cone photoreceptors. *Opt Express.* 2010; 18:5257–5270. [PubMed: 20389538]
85. Srinivasan VJ, Monson BK, Wojtkowski M, et al. Characterization of outer retinal morphology with high-speed, ultrahigh-resolution optical coherence tomography. *Invest Ophthalmol Vis Sci.* 2008; 49:1571–1579. [PubMed: 18385077]
86. Zhang Y, Cense B, Rha J, et al. High-speed volumetric imaging of cone photoreceptors with adaptive optics spectral-domain optical coherence tomography. *Opt Express.* 2006; 14:4380–4394. [PubMed: 19096730]
87. Fuerst NM, Serrano L, Han G, et al. Detailed functional and structural phenotype of Bietti crystalline dystrophy associated with mutations in CYP4V2 complicated by choroidal neovascularization. *Ophthalmic Genet.* 2016; 37:445–452. [PubMed: 27028354]
88. Mohammad S, Gottlob I, Kumar A, et al. The functional significance of foveal abnormalities in albinism measured using spectral-domain optical coherence tomography. *Ophthalmology.* 2011; 118:1645–1652. [PubMed: 21570122]

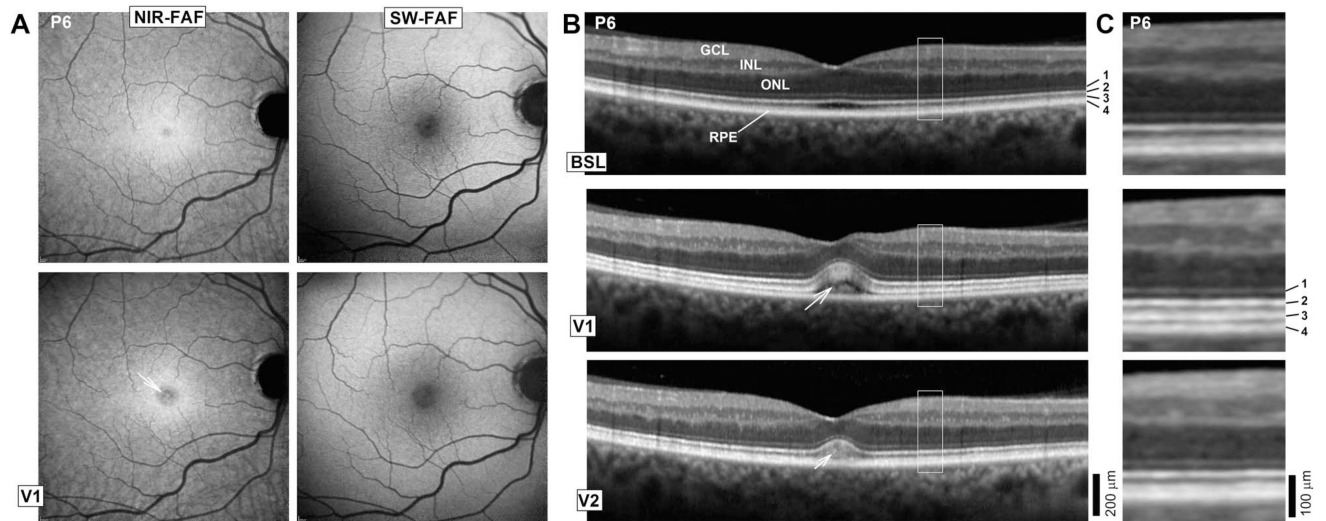


Fig. 1.

A. En face retinal imaging of the RPE melanin content using NIR-FAF, and lipofuscin content with SW-FAF in a patient with the most prominent abnormalities. Images were obtained at baseline (BSL) and at a visit (V1), when retinal changes were first noted. Arrow in NIR-FAF V1 points to the foveal center. **B.** Six millimeter long horizontal SD-OCT cross-sections through the fovea in the patient at BSL, V1, and 6 days (V2) after discontinuation of the study medications because of systemic side effects. Nuclear layers are labeled (outer nuclear layer [ONL]; inner nuclear layer [INL]; ganglion cell layer [GCL]). Outer photoreceptor/RPE laminae are numbered to the side of the BSL image: 1, ELM; 2, EZ; 3, IZ; and 4, RPE/BrM. **C.** Magnified images corresponding to regions delimited by white squares in (B) show details of the outer photoreceptor and RPE/BrM structure.

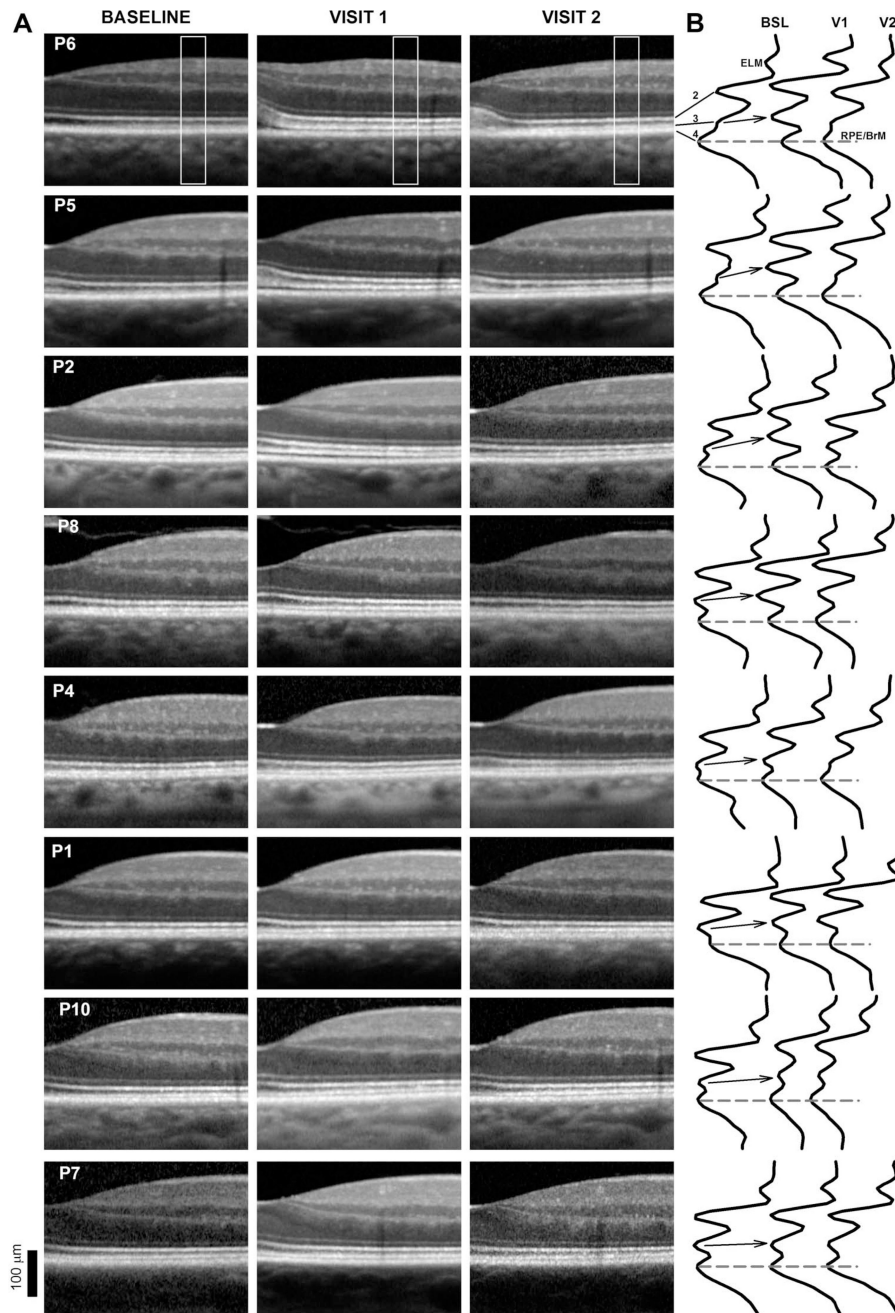


Fig. 2.

A. Spectral domain OCT cross-sections from the fovea to 1.4 mm in the nasal retina in 8 of the patients at baseline (BSL), Visit 1 (V1, 30 days posttreatment initiation), and Visit 2 (V2, 180 days posttreatment, 6 days after treatment discontinuation for P6). Patients are ordered from top to bottom by the magnitude of the structural abnormalities. Only the right eye shown for clarity. **B.** Longitudinal reflectivity profiles obtained from the region area (0.9 mm in the nasal retina) boxed in (A). Longitudinal reflectivity profiles are normalized to the RPE/BrM signal amplitude. Dashed lines connecting RPE/BrM peaks provide a reference; arrows visually connect the location of the IZ signal from baseline to Visit 1 (V1).

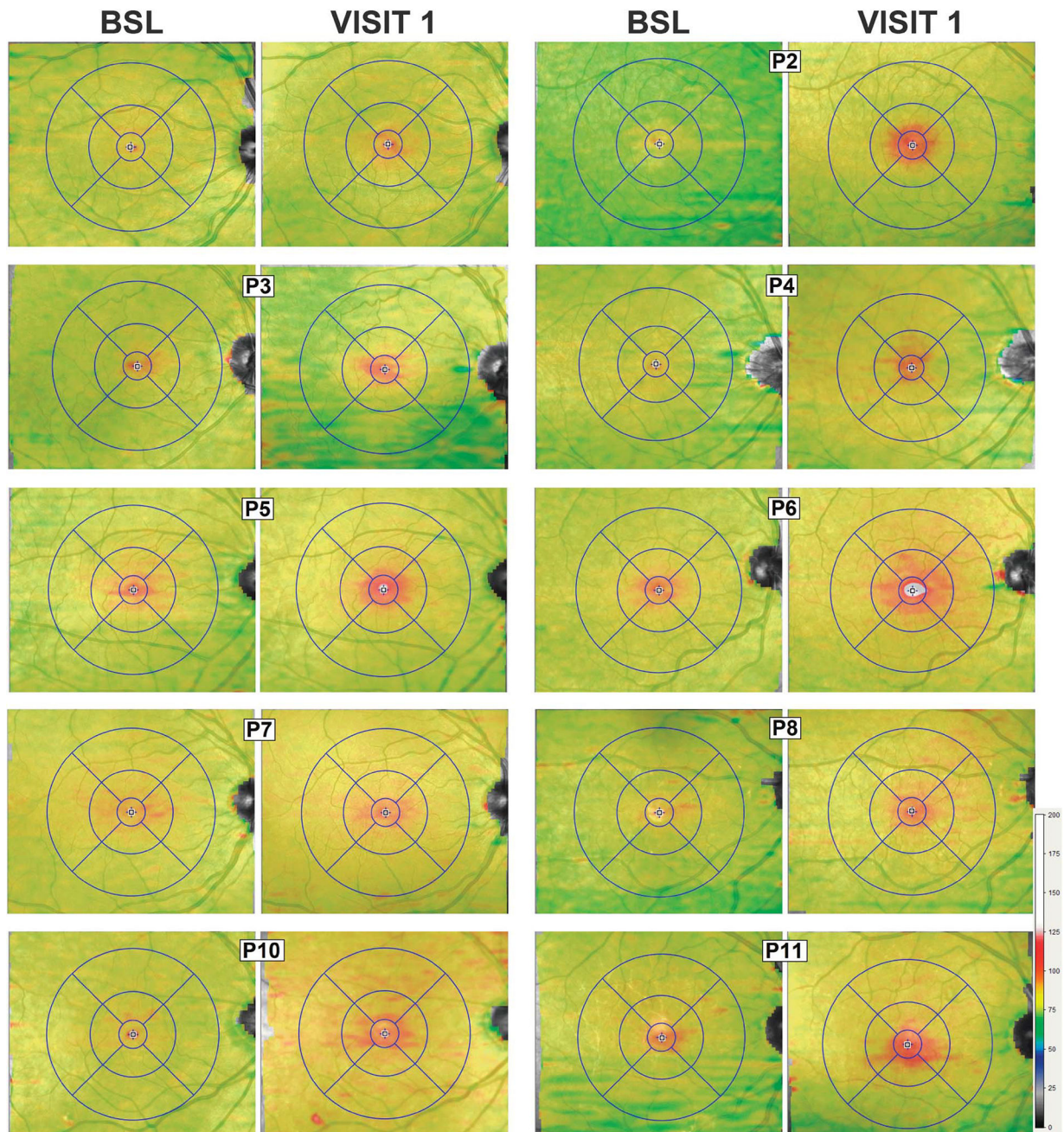


Fig. 3. Topography of the outer retina changes after MEK/BRAF inhibition. Shown are $30^{\circ} \times 25^{\circ}$ topography maps of the distance (or thickness) between the internal limiting membrane and the RPE/BrM layer defined by SD-OCT in 8 of the patients at their baseline (BSL) visits compared with a visit (V1) ~30 days after initiation of the clinical trial medications. Only the right eye shown for clarity. Thickness values (in μm) are mapped to a color scale (bottom right). Superimposed is an early treatment diabetic retinopathy study grid centered at the foveola. Concentric circles of increasing radii divide the central macula in subfields: Central (500 μm radius), inner parafoveal (1,500 μm), and outer parafoveal (3,000 μm).

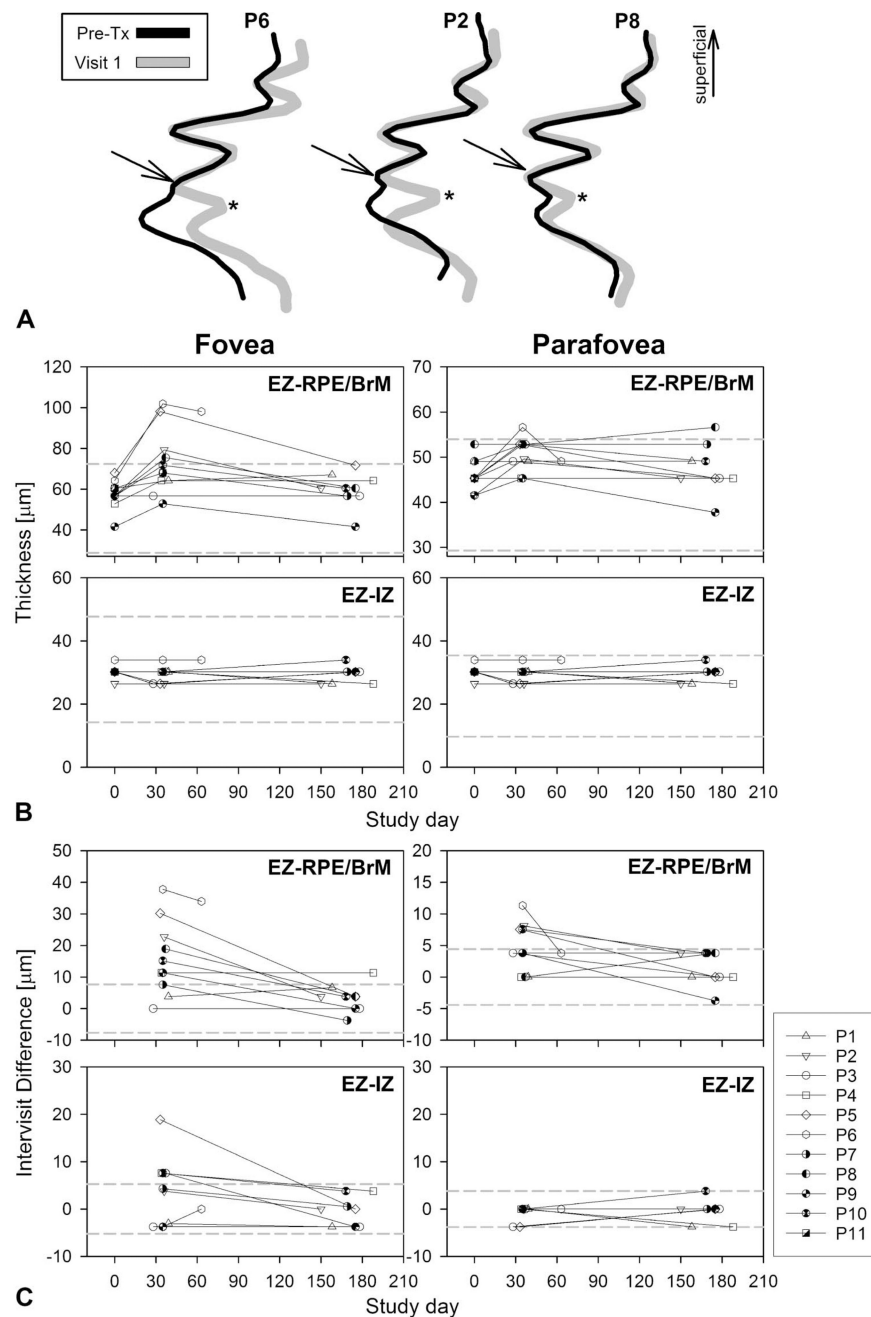


Fig. 4. Timecourse of the structural changes. **A.** Longitudinal reflectivity profiles of the outer retinal sublaminae obtained from the nasal parafovea pretreatment (Pre-TX) are overlaid on LRP from visit 1 (gray traces), ~30 days after medication onset of representative patients. Arrows point to the IZ signal peak as an independent component separated by a trough (asterisk) from the RPE. The traces overlap perfectly in the segment between the EZ and the IZ supporting no changes in POS length. **B.** Timecourse of the foveal and parafoveal (1.5 mm of eccentricity) changes in thickness for the EZ-to-RPE/BrM and EZ-to-IZ layer distances. The latter relates to the length of the POS. Dashed lines are normal mean \pm 2 SD ($n = 68$,

ages 8–61 years). **C.** Timecourse of the foveal and parafoveal (1.5 mm of eccentricity in the nasal retina) thickness expressed as a difference between the value on a given study date and measurements pretreatment. Dashed lines define mean \pm 2 SD of the intervisit variability of the parameter determined at baseline visits and in normal subjects.

Table 1

Clinical Characteristic of Patients

Study ID	Age at Enrollment		Visual Acuity* Baseline		Visual Acuity* Follow-up [‡]		Refraction [‡]		Foveal Sensitivity Baseline (dB)		Foveal Sensitivity Follow-up (dB) [‡]		Mean Defect Baseline (dB)		Mean Defect Follow-up (dB) [‡]	
	RE	LE	RE	LE	RE	LE	RE	LE	RE	LE	RE	LE	RE	LE	RE	LE
P1	20/20	20/20	20/20	20/20	20/20	20/20	Plano	Plano	34	34	38	38	-1.70	-1.44	+1.20	+1.02
P2	20/20	20/20	20/20	20/20	20/20	20/20	-0.25	+0.12	36	36	na	na	+1.40	+0.91	+1.61	+1.13
P3	20/20	20/20	20/20	20/20	20/20	20/20	+0.50	+0.50	na	na	na	na	-0.08	-0.59	-3.75	-3.54
P4	20/20	20/20	20/20	20/20	20/20	20/20	-6.25	-6.75	29	31	na	na	na	na	+2.16	+1.48
P5	20/20	20/20	20/20	20/20	20/20	20/20	+1.00	+1.00	37	37	32	34	+1.57	+1.37	+0.06	+0.10
P6	20/20	20/20	20/20	20/20	20/20	20/20	-1.00	Plano	na	na	34	32	+1.47	+0.84	+1.59	+1.31
P7	20/20	20/20	20/20	20/20	20/20	20/20	-0.25	Plano	33	33	35	34	-1.34	-2.32	-1.34	-1.68
P8	20/20	20/20	20/20	20/20	20/20	20/20	+0.25	+0.75	na	na	32	36	-0.04	+0.29	+0.88	+0.85
P9	20/40	20/20	20/25	20/20	20/25	20/20	+2.00	+2.00	na	na	31	33	-0.93	-0.71	-2.78	-1.57
P10 [§]	20/20	20/25	20/20	20/25	20/20	20/25	+1.75	+2.00	35	28	38	30	-3.77	-23.59	+0.50	-17.07
P11	20/20	20/20	20/20	20/20	20/20	20/20	-0.25	+0.12	33	34	na	na	-0.52	-0.04	na	na

* Best-corrected visual acuity.

[‡] Spherical equivalent.

[‡] Follow-ups are at the 6-month visit (range 150–188 days) except P6 which was at the 1-month visit, before treatment discontinuation. Normal mean foveal sensitivity \pm 2 SD = 38 ± 6 dB.

[§] P10 carries a diagnosis of open-angle glaucoma with a dense arcuate visual field defect, both eyes.

LE, left eye; na, not available/not performed; RE, right eye.